



1 **Inversion, Assessment of Stability and Uncertainty of Geoelectric Sounding data**
2 **using a New Hybrid Meta-heuristic algorithm and Posterior Probability Density**
3 **Function Approach**

4 Kuldeep Sarkar, Upendra K. Singh*

5 Department of Applied Geophysics, IIT (ISM), Dhanbad 826004, Jharkhand, India

6 *Correspondence: upendra@iitism.ac.in

7 **ABSTRACT**

8 Estimating a reliable subsurface resistivity structure using conventional techniques is
9 challenging due to the nonlinear nature of the inverse problems. The performance of the
10 inversion techniques can be pretty ambiguous based on the optimal error. Although
11 traditional methods have proven to be quite effective. The impact of the constraints accessible
12 from the borehole is examined for further assessment and enhance the algorithm's
13 effectiveness. The vPSOGWO is a new approach based on model search space without any
14 prior information. This new strategy describes the hybridization of the particle swarm
15 optimizer (PSO) with the grey wolf optimizer (GWO). To understand the efficiency and
16 novelty of the algorithm, it has been validated on two different kinds of synthetic resistivity
17 data with various sets of noise and finally applied on three field datasets of different
18 geological terrains. The analyzed results suggest that the subsurface resistivity model shows
19 considerable uncertainty. Thus, it is superior to examine the histograms and posterior
20 probability density functions (PDF) of such solutions for exemplifying the global solution.
21 PDF with 68.27% CI selects a region with a higher probability. Therefore, the inverted
22 models are used to estimate the mean global solution and the most negligible uncertainties,
23 where the mean global solution represents the best solution. Our vPSOGWO inverted
24 outcomes have been proven to be more accurate than classic PSO, GWO and state-of-art



25 variant of classic approaches. As a results, this novel method plays a vital role in DC data
26 inversion effectively.

27 **Keywords:** vPSOGWO, Uncertainty, Stability, Inversion, Resistivity data.

28

29 1. INTRODUCTION

30 The vertical electrical resistivity sounding (VES) method is an economical and simple
31 method due to a wide application such as hydrogeological, groundwater, minerals,
32 geothermal, hydrocarbon, engineering, environmental fields, etc. (Sen et al., 1993, Sharma,
33 2012, Panda et al., 2018), which have been used for determining the layered parameters. The
34 VES data interpretation is challenging due to its unstable, nonunique solution and algorithm
35 sensitivity (Narayan et al., 1994, Oldenburg and Li, 1994, Singh et al., 2005, 2013).
36 Therefore, many researchers have developed several inversion algorithms to improve the
37 accuracy, stability and reduce the uncertainty of the solutions. These inversion techniques are
38 grouped into local and global optimization techniques. In the local inversion techniques, a
39 logical initial guess is required to get the solution. The researchers have led to think about
40 alternative methods, where a broad range of parameters can be established. Many researchers
41 have developed various metaheuristic optimization algorithms to solve various real-world
42 problems. These algorithms inspired from the natural phenomenon include Ant Colony
43 (Colorni et al., 1991), Bat algorithm (Yang, 2010), Biogeographically based Optimization
44 (Simon, 2008), Differential Evolution (Storn and Price, 1997), Firefly algorithm (Yang,
45 2010), Genetic Algorithm (Whitley, 1994; Mitchell, 1996), Gravitational Search Algorithm
46 (Rashedi et al., 2009), Grey Wolves Optimizer (Mirjalili et al., 2014), Particle Swarm
47 Optimization (Kennedy and Eberhart, 1995), etc. These optimization techniques aim to have
48 an optimum solution and fast convergent rate to obtain global minima. However, unique
49 characteristics, viz. exploration and exploitation, in global optimization algorithms persist.



50 For example, the Particle Swarm Optimization (PSO) algorithm has very high potential in
51 exploitation, implies that the algorithm performs well in local search (Senel et al., 2019) but
52 is inferior in exploration, which means the algorithm has less ability to find out the starting
53 position near-global minima and because of low exploration characteristics, it gets trapped at
54 the local minima (Eiben and Schippers, 1998, Mirjalili and Hashim, 2010). So, integrating the
55 two algorithms with opposite characteristics is the best way to solve the exploration
56 characteristics and exploitation characteristics, and provide more accurate and reliable
57 solution than results obtained from an individual's algorithm. Many authors have developed
58 various hybrid metaheuristic algorithms such as PSOGA for fundamental function analysis,
59 PSOACO for data mining, PSODE for global optimization using the standard function, and
60 PSOGSA using the standard function (Esmin et al., 2013; Lai and Mingyi, 2009; Rashedi et
61 al., 2009).

62 This study focuses on a variable weight hybrid algorithm that fuses the exploration
63 ability of Particle Swarm Optimizer (PSO) with the exploration ability of Grey Wolves
64 Optimizer (GWO), known as vPSOGWO (Şenel et al., 2019). In this algorithm, some
65 random particles of PSO are replaced by the new ones obtained from GWO. Earlier the
66 constant weight hybrid technique of PSO and GWO known as HPSOGWO has been used
67 in different applications by some authors, such as for single area unit commitment
68 problems (Kamboj, 2015), mathematical problems (Singh and Singh, 2017), and
69 benchmark functions and real-world issues (Senel et al., 2019). But none of the researchers
70 have tested the current work in geophysical data inversion to the best of our information.
71 Thus, the applicability of the vPSOGWO algorithm is demonstrated on synthetic data with
72 noise, without noise, and various field resistivity sounding data for estimating the
73 resistivity distribution in a 1D earth's subsurface model. The study also calculate the
74 posterior probability density functions (PDF) with 68.27% confidence interval and



75 correlation matrix on all accepted models for determining mean global model and
76 uncertainty. As a result, we analysed and compared the effectiveness of the proposed
77 algorithms with classical PSO, GWO and state-of-art variant of classic methods. Our
78 analysis advocates that the vPSOGWO algorithm produces a more accurate and reliable
79 model with excellent stabilities and the least uncertainty in the model independently, as
80 well as the ability to successfully resist noise.

81

82 2. FORWARD MODELLING ALGORITHM

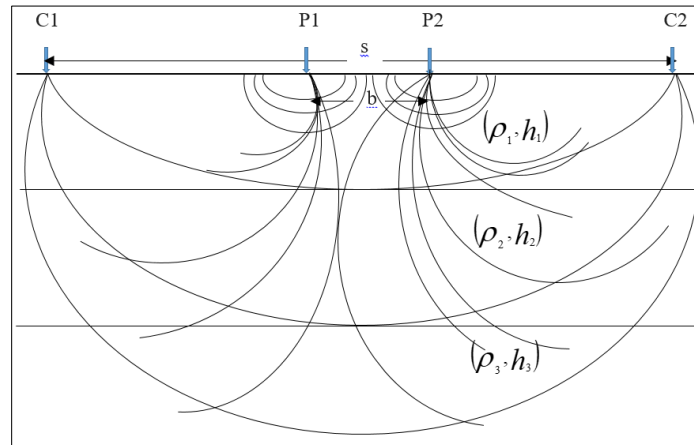
83 The forward code is developed, and synthetic resistivity data sets were created using the
84 kernel function (Koefoed, 1979) with Schlumberger resistivity configuration (*Fig. 1*) from
85 known parameters such as current electrode spacing, number of geological multilayers of
86 true resistivity their thickness. The mathematical expression for apparent resistivity is
87 given as:

$$88 \quad \rho_a(s, \mathbf{m}) = \rho_1 + s^2 \rho_1 \int_0^\infty T_1(\lambda, \mathbf{m}) J_1(\lambda s) d\lambda \quad (1)$$

89 where, J_1 is the first order Bessel function, λ is the integration variables, s is half of the
90 current electrode spacing, \mathbf{m} is the model. T_n is the kernel's resistivity transform, ρ_k is the
91 resistivity and t_k is the thickness of the k^{th} layers.

92 For each layer, the kernel's resistivity transform T_k has been determined by Pekeris
93 (1940). The apparent resistivity, $T_k(\lambda)$, is convolution with linear filter theory to compute
94 as:

$$95 \quad T_k(\lambda) = \rho_k * (T_{k+1}(\lambda) + \rho_k \tanh(\lambda t_k)) / (\rho_k + T_{k+1}(\lambda) \tanh(\lambda t_k)) \quad (2)$$



96

97 **Figure 1.** Schlumberger array configuration for three layer case, where C1 and C2, through
98 which current is injected, are current electrode with spacing s ; P1 and P2 are potential
99 electrodes with spacing b .

100

101 3. INVERSE MODELLING ALGORITHM

102 The geophysical inverse problem can be formulated through forward modelling
103 operator/functional to aim at achieving the geophysical model/solution, which illuminates the
104 observed data in the best. This operator integrates the geophysical problems and maps
105 between the observed data y and the solution x as:

$$106 \quad y = f(x) \quad (3)$$

107 Inversion set up finding a model that minimizes cost function/misfit functional that generally
108 is a degree of the relationship between the N number of observed data (y_o) and the calculated
109 data (y_c). This misfit functional can be introduced here as a mean-square-error (MSE) and
110 can be defined as:

$$111 \quad \text{MSE} = \frac{1}{N} \sum_{i=1}^N (y_o - y_c)^2 \quad (4)$$

112



113 **3.1. Particle swarm optimization**

114 Particle swarm optimization (PSO) is based on the social behavior of animals such as
115 schooling of fish or flocking of bird (Kennedy and Eberhart in 1995). When the birds go in
116 search of food, they scattered randomly within the search space before they can determine
117 the position of food. While searching for food, there is always a bird who is aware of the
118 position of food. This information they share with others. In this method, each bird is
119 called as particle which is represented by geophysical solutions/models (i.e., here particle
120 is resistivity layer parameters). The capability/fitness of each swarm/birds is estimated
121 between the N number of observed data (y_o), which measure the swarm and the food
122 distance, and the computed data (y_c) which measures the swarm and the estimated position
123 (resistivity layer parameter/solution) of the prey distance using equation 4.

124 The best position among particles with information about it are store for each
125 iteration in memory. The new velocity and position of the population pool are accepted if
126 its possibility is large, otherwise it is rejected. In that case, the particles are randomly
127 distributed in the search space in order to escape the local optima. The search continues
128 until it gains maximum possibility or it reaches the maximum iteration. In global search
129 space, the position of each particle is updated by the following two mathematical
130 equations:

131
$$\vec{v}_i(t+1) = \vec{v}_i(t) + c_1 \times rand(\vec{x}_p(t) - \vec{x}_i(t)) + c_2 \times rand(\vec{x}_g - \vec{x}_i(t)) \quad (5)$$

132
$$\vec{x}_i(t+1) = \vec{x}_i(t) + \vec{v}_i(t+1) \quad (6)$$

133 Here, \vec{v}_i represent the velocity of the i^{th} particle with position \vec{x}_i , \vec{x}_p is the best
134 position obtained by the i^{th} particle, \vec{x}_g is the best position, t is the number of the iteration,
135 i represents the number of the model ($i = 1, 2, 3, \dots, N$), $rand$ represent the random values
136 with range [0,1], and the coefficient c_1 and c_2 represent the optimization parameter. The



137 disadvantage of PSO algorithm is that, while directing particles to random positions, it has
138 small possibility to escape the local minima.

139

140 **3.2 Grey wolf optimization**

141 Grey wolf optimization (GWO) algorithm mimics the leadership hierarchy and hunting
142 mechanics of grey wolves, and used its ability to solve the standard and real-life problems. In
143 the grey wolf's community, they are divided in four groups: (i) the alpha, (ii) the beta, (iii)
144 the delta and (iv) the omega, in which alpha, beta and delta are the fittest wolves, who guide
145 omega towards promising areas of the search space. The alpha is the leader, which generally
146 makes important and final decision for all the wolves so and represents the fittest solution.
147 The betas are subordinates that help the alphas in their decision making but they cannot force
148 them in any decision. They can only order the lower wolves. The beta group takes the order
149 from alpha group which they reinforce throughout the other group and send back the
150 feedback to the alpha. All the groups dominate over the omega wolves. The omega group is
151 an important part during hunting as they play role of the scapegoat and are always allowed to
152 eat at the end. If a wolf is not the part of alpha, beta or omega group, then they are known as
153 delta which only submit to alpha and beta groups. In GWO algorithm, the alpha group
154 represents the best position, i.e., geophysical model/solution. In our case geophysical model
155 is resistivity layer parameters. The beta and delta groups are consecutive best solutions and
156 omega group is the best solution that follows always the other groups. The capability/fitness
157 of each wolf is estimated between the observed data (which measures wolf and prey distance)
158 and the computed data (which measures the wolf and the estimated position of the prey
159 distance) using equation 4.



160 Hunting in the grey wolf's community has been divided into three groups: prey
161 search, encircling the prey, and attacking the prey. The encircling nature of the wolves is
162 defined by the following equation:

$$163 \quad d = |c \times (t) - \vec{x}_i(t)| \quad (7)$$

$$164 \quad \vec{x}_i(t + 1) = \vec{x}_p(t) - a \times d \quad (8)$$

165 where, \vec{x}_p is the prey position, \vec{x}_i is the grey wolf's positions, a and c are the vectors
166 mathematically formulated as:

$$167 \quad a = a_1 \times (2 \times rand - 1) \quad (9)$$

$$168 \quad c = 2 \times rand \quad (10)$$

169 Here, $a_1 = 2 \times (1 - t/l)$ which varies from 2 to 0 in decreasing order with
170 increasing iteration (t), l represent the maximum iteration, and $rand$ is the random
171 number between [0,1].

172 The alpha group led the grey wolves' community, in which the beta and the delta
173 group to search the prey location and the omega groups follow them. The alpha group
174 wolves gives the best solution, while the second and third best solution is provided by
175 the beta and the delta group wolves, respectively. Therefore, the rest community wolves
176 i.e., omega group wolves follows the best solution wolves to obtain best location. This is
177 mathematical equated by:

$$178 \quad d_{\alpha,\beta,\delta} = |\vec{c}_{1,2,3} \times \vec{x}_{\alpha,\beta,\delta} - \vec{x}| \quad (11)$$

179 The best location/position for alpha, beta and delta wolves in each iteration is
180 given by \vec{x}_α , \vec{x}_β and \vec{x}_δ , respectively.

$$181 \quad \vec{x}_{1,2,3} = |\vec{x}_{\alpha,\beta,\delta} - \vec{a}_{1,2,3} \times \vec{d}_{\alpha,\beta,\delta}| \quad (12)$$

182 Here, $\vec{x}_p(t + 1)$ describe the updated position of the prey in ($t + 1$) iteration
183 which is obtained from the mean position of three best wolves in the population, that is,

$$184 \quad \vec{x}_p(t + 1) = (\vec{x}_1 + \vec{x}_2 + \vec{x}_3)/3 \quad (13)$$



185 The values of a are utilized by wolves which force the search to move away from
186 the prey. When $a \geq 1$, the hunting is abandoned in order to have a better solution and,
187 when $a < 1$, the wolves are enforced to attack the prey. In equation 9, a varies between
188 $[-2a_1, 2a_1]$.

189

190 **3.3 Hybrid variable weighted PSOGWO (vPSOGWO)**

191 Despite its usefulness in achieving successful results in real-world problems, it tends to
192 fall into the local minima, causing the solution to move away from global minima. This
193 tendency for deteriorating within the local minima is stopped by the exploration ability
194 of the GWO algorithm. Therefore, the hybrid variable weighted PSOGWO, known as
195 vPSOGWO that fuses the exploitation potential of PSO with the exploration potential of
196 GWO to overcome each other's discrepancy with the implementation of varying weight.
197 Due to the involvement of two distinct variants running together to solve the problem,
198 this hybrid vPSOGWO is called a co-evolutionary hybrid algorithm. The encircling
199 behaviour of each wolf is updated by the following equations:

$$200 \quad \vec{d}_{\alpha,\beta,\delta} = |\vec{c}_{1,2,3} \times \vec{x}_{\alpha,\beta,\delta} - w \times \vec{x}| \quad (14)$$

$$201 \quad \text{Here, } w = w_{max} - (w_{max} - w_{min}) \times t/l \quad (15)$$

202 Here, $w_{max} = 0.9$, and $w_{min} = 0.2$ are found more appropriate after tuning for our
203 study.

204 The best location/position (geophysical model) for alpha, beta and delta wolves in
205 each iteration is given by \vec{x}_α , \vec{x}_β and \vec{x}_δ , respectively.

$$206 \quad \vec{x}_{1,2,3} = |\vec{x}_{\alpha,\beta,\delta} - \vec{a}_{1,2,3} \times \vec{d}_{\alpha,\beta,\delta}| \quad (16)$$

207 where,

$$208 \quad a_{1,2,3} = a_1 * (2 * rand - 1) \quad (17)$$

$$209 \quad c_{1,2,3} = 0.5 \text{ (chosen after tuning)} \quad (18)$$



210 $a_1 = 2 * (1 - t/l)$ (19)

211 The updated velocity and position of vPSOGWO are:

212 $\vec{v}_i(t + 1) = w \times \vec{v}_i(t) + c_1 \times rand \times (\vec{x}_1 - \vec{x}_i(t)) + c_2 \times rand \times (\vec{x}_2 - \vec{x}_i(t)) +$
213 $c_3 \times rand \times (\vec{x}_3 - \vec{x}_i(t))$
214 (20)

215 $\vec{x}_i(t + 1) = \vec{x}_i(t) + \vec{v}_i(t + 1)$ (21)

216 Here, the value 1.5 for each coefficients $c_1, c_2,$ and c_3 after tuning the parameters
217 found more suitable in the present study (Roshan and Singh, 2017).

218

219 **vPSOGWO algorithm**

220
221 *Max_Iter*: maximum iterations set

222 *Pop_no*: population size

223 *Para*: Number of parameters

224 *Fitness=infinite*: already set

225 *Lb* and *Ub*: set Lower bound (*Lb*) and Upper bound (*Ub*) for different parameters

226 *Initialize particles randomly*

227 Procedure

228 for $l = 1$ to *Max_Iter* do

229 for $i = 1$ to *Pop_no* do

230 for $j = 1$ to *Para* do

231 check the *Lb* and *Ub* for randomly created particles

232 end

233 end

234 for $i = 1$ to *Pop_no* do



```
235         Calculate the fitness form cost function
236         Update the wolves' fitness and position
237     end
238     Update a1, a, c, w, using equations (15-17), (13)
239     for i = 1 to Pop_no do
240         for j = 1 to Para do
241             Update position of  $\vec{x}_1$ ,  $\vec{x}_2$  and  $\vec{x}_3$  using equations (14) and (16)
242             Update best particle velocity and position using equations (20-21)
243         end
244     end
245 end
246
```

247 **4.0 Statistical simulation for global model and uncertainty estimation**

248 The proposed algorithms yield good-fitting models, but the evaluation of a global solution
249 requires numerous techniques. It is noteworthy for selecting the region of solution/model
250 search space, where we find enormous solutions. The methods for selecting the region of
251 model space were selected to envisage the global solution and reduce the uncertainty in the
252 ultimate solution (Mosegaard and Tarantola, 1995; Sen and Stoffa, 1996). Thus, many
253 solutions and associated error estimated were kept in memory for consequent statistical
254 measurements. Therefore, 10^8 solutions were generated for each algorithm using logarithmic
255 mean square error, and every computed response corresponding to each model fits well with
256 the observed response. However, the model parameters obtained may differ from each other,
257 which lie within the search range in multidimensional space. Hence, the mean model from the
258 model parameters is defined as (Ross, 2009):

$$259 \quad \hat{\mathbf{m}}_i = \frac{1}{M} \sum_{j=1}^M \mathbf{m}_{i,j} \quad (20)$$



260 where $i = 1$ to the total number of the parameters, M is the total models and $\mathbf{m}_{i,j}$.

261 All algorithms are executed for 10,000 runs with 1000 iterations to obtain the best
262 model parameters. It is noteworthy to mention that in vPSOGWO, multiple runs are crucial
263 because 1000 weightage points are laying in between the inertial weights of 0.9 to 0.2, such
264 that each weightage point yields a fitted model in a run. As a result, 10,000 runs provide
265 10,000 chances to each weightage point to fetch the best-fitted model.

266 Therefore, the posterior covariance matrices are defined in the equation (Ross,
267 2009):

$$268 \quad Cov(\mathbf{m}_{i,k}) = \frac{1}{M-1} \sum_{j=1}^M (\mathbf{m}_{i,j} - \hat{\mathbf{m}}_i) \times (\mathbf{m}_{k,j} - \hat{\mathbf{m}}_k) \quad (21)$$

269 and posterior correlation matrices are described in the equation:

$$270 \quad Corr(\mathbf{m}_{i,k}) = Cov(\mathbf{m}_{i,k}) / \sqrt{Cov(\mathbf{m}_{i,i}) \times Cov(\mathbf{m}_{k,k})} \quad (22)$$

271 where i and k lie between 1 to total number of parameters.

272 The square-rooted diagonal elements of the covariance matrix define the
273 uncertainty of the solution, and the correlation matrix gives a rough idea about the relation
274 between the model parameters. If the parameters don't provide a global solution, then the
275 apparent resistivity curve corresponding to the mean model will not adequate the observed
276 value. The posterior correlation matrix corresponding to the indigenous solution will not
277 yield an actual correlation between the parameters obtained via linear regression. For
278 further analysis, posterior PDF and histogram are calculated over all accepted models. The
279 one-dimensional posterior probability density function for various parameters with mean
280 $\hat{\mathbf{m}}_i$ and standard deviation σ_i is given as (Ross, 2009):

$$281 \quad p(\mathbf{y}_i, \hat{\mathbf{m}}_i, \sigma_i) = (1/\sigma_i \sqrt{2\pi}) \times \exp(-(\mathbf{y}_i - \hat{\mathbf{m}}_i)^2 / 2\sigma_i^2) \quad (23)$$

282 where y is the solution/model parameter's output store after 10,000 runs of an algorithm
283 and $i = 1$ to the number of model parameters.



284 Different techniques are based on the posterior PDF to obtain the global solution.
285 One of the techniques is to pick the model parameters with the highest probability values.
286 Another method based on PDF is to normalize (0 to 1) each model parameter by their
287 respective highest probability values. The best model is considered to have the highest sum
288 of normalized probability values (Sharma, 2012). Further, the best model can also be
289 determined by taking the mean of each parameter with probably more significance than the
290 threshold probability. However, these techniques fail to provide the global model.

291 Therefore, proceeding with a new approach to the study by introducing a
292 confidence interval (CI) more significant than 68.27% as a benchmark for all model
293 parameters. According to the empirical rule, 68.27% of the data lies within the one
294 standard deviation of the mean (Ross, 2009). Thus, the model parameters below 68.27% CI
295 are discarded, and the remaining parameters are used for determining the mean solution
296 and uncertainty. It means that the model represents the global solution with less
297 uncertainty.

298

299 **5.0 Computation information**

300 The code was developed in MATLAB R2019a in Windows 10 platform having
301 configuration: Model-HP Z240 Tower Workstation, Processor- Intel Xeon CPU E3-1225
302 v6 @ 3.30GHz, 32.0 GB RAM, 64-bit operating system (OS). However, Global
303 optimization is a time-consuming process, as it requires many forwarding calculations to
304 obtain the best-fitted result.

305

306 **6.0 Results and discussion**

307 The applicability of the new algorithm vPSOGWO, GWO, and PSO has been assessed
308 inverting several cases of synthetic and field data extracted from different geological

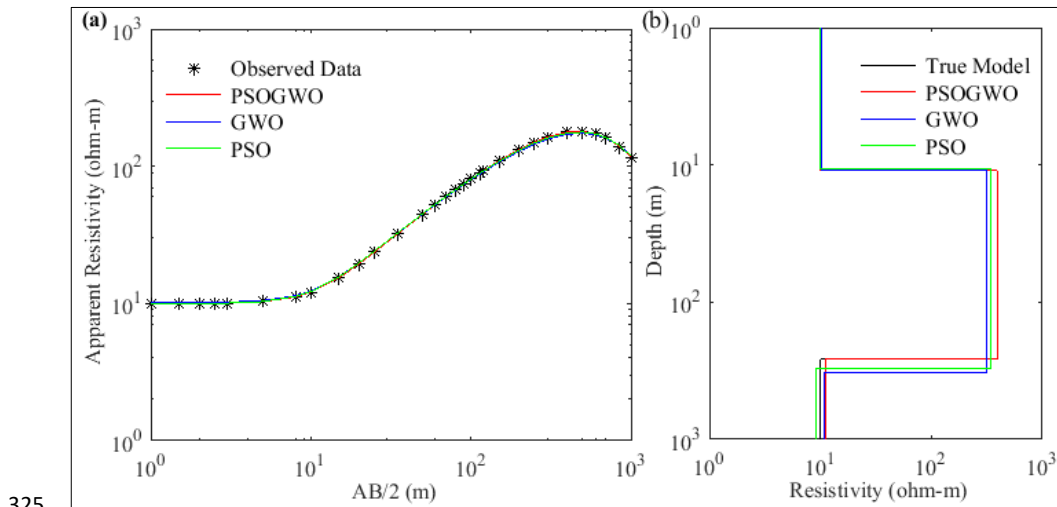


309 terrains (Dixon & Doherty, 1977; Panda et al., 2017). Both synthetic and field data sets
310 were computed and optimized using the developed algorithms, keeping the ten population
311 size and 1000 iterations for 10,000 runs, leading each algorithm to analyzed 10^8 models.
312 We have discussed the inverted results of algorithms to the application on few examples of
313 synthetic and field cases:

314

315 6.1 Example 1: Synthetic data- Three-layer case

316 Initially, to access the applicability and efficacy of the proposed algorithms, a synthetic
317 apparent resistivity sounding data measured with Schlumberger array is generated
318 considering the three-layered earth model sandwich with a high resistive layer of $500.0\Omega\text{m}$
319 and thickness 150.0 m between two low resistive layers of $8.0\Omega\text{m}$ and $5.0\Omega\text{m}$. The
320 synthetic data is computed in the Matlab environment as shown in *Fig. 2(a)* with the (*)
321 mark. *Fig. 2* shows (a) the three-layer synthetic data with the best fitted calculated apparent
322 resistivity curve ($> 68.27\%$ PDF) and (b) one-dimensional mean model ($> 68.27\%$ PDF)
323 for true model (black color), vPSOGWO (red color), GWO (blue color) and PSO (green
324 color).

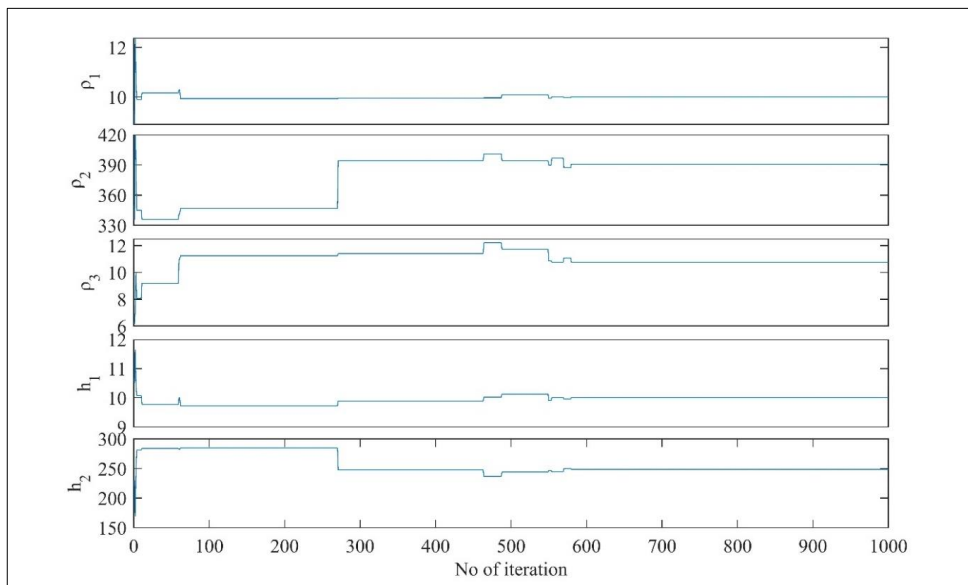




326 **Figure 2.** Three layer synthetic data (a) observed (*) and the best fitted calculated apparent
327 resistivity curve (> 68.27% PDF); (b) one dimensional mean model (> 68.27% PDF) for true
328 model (black colour), vPSOGWO (red colour), GWO (blue colour) and PSO (green colour).

329

330 The search limit for novel inversions techniques (vPSOGWO, GWO, and PSO) is
331 carefully chosen, as shown in *Table 1*. Each algorithm, including vPSOGWO, runs 10,000
332 times to perform statistical analysis and determine the global mean model with the least
333 uncertainty. *Fig. 3* shows the convergence curve of the resistivity layer parameters using
334 vPSOGWO. We found no changes seen in the convergence pattern after 590 iterations, and
335 layer parameters get stable. The convergence curves in terms of error versus iterations for
336 existed three algorithms are shown in *Fig. 4*. It is observed that vPSOGWO, GWO, and
337 PSO have converged at 590, 950, and 380 iterations with the mean square error of $1.586e-$
338 8 , $5.238e-8$, and $5.792e-8$, respectively, whereas ridge regression has an error of 0.633.

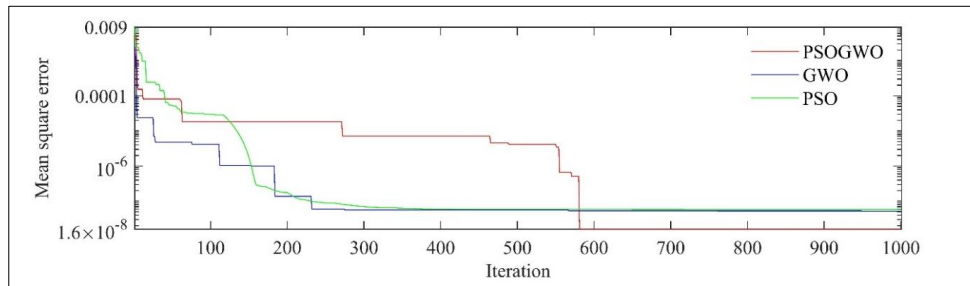


339

340 **Figure 3.** Convergence curve for best fitted model parameters for vPSOGWO algorithm.

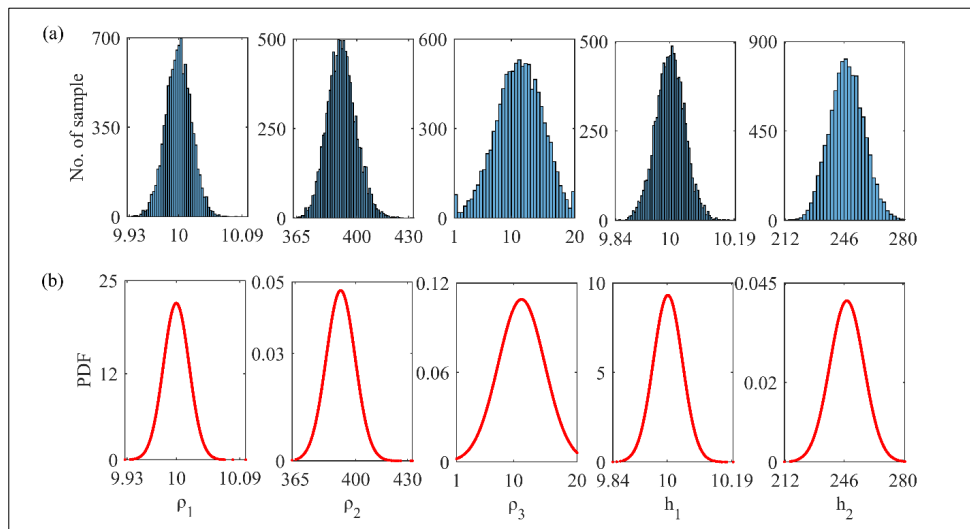


341



342

343 **Figure 4.** Convergent curve known as error versus iteration curve for three layers noiseless
344 synthetic data.



345

346 **Figure 5.** (a) Histogram and (b) posterior PDF of all 10,000 solution corresponding to
347 output of each run for three layer synthetic earth model.

348

349 The 10,000 models inverted are used to find out the posterior PDF and histogram
350 for each parameter. As shown in *Fig. 5(a)*, the peak of posterior PDF is roughly close to the
351 actual model parameter. The histogram is shown in *Fig. 5(b)* suggests that the ρ_2 and h_2



352 have a broader range. It represents the equivalence problem associated with the resistive
 353 layer as the uncertainty in each algorithm was found to be large considering all the
 354 accepted models. So by selecting the models having posterior PDF greater than 68.27% CI
 355 reduces the uncertainty in the model, increases the resolution of a solution, and helps
 356 estimate the best mean model close to the actual model (*Table 1*). *Table 1* shows the model
 357 parameters and uncertainty for proposed algorithms.

358 **Table 1.** Optimization mean model result for three layer synthetic resistivity sounding data.

Model Parameter	True value	Search Range	True model	Mean model (final 10000 solution)			Mean model (PDF > 68.27%)		
				GWO	PSO	vPSOGWO	GWO	PSO	vPSOGWO
				ρ_1 (Ωm)	10	5 – 15	10 ± 0.06	10.33 ± 0.55	10 ± 0.39
ρ_2 (Ωm)	390	15 – 500	398 ± 8.2	324.55 ± 56.71	343.10 ± 49.70	391.29 ± 8.39	319.15 ± 24.02	340.90 ± 23.10	391.09 ± 3.67
ρ_3 (Ωm)	10	1 – 20	10 ± 0.05	10.50 ± 3.76	9.56 ± 7.78	11.25 ± 3.66	10.71 ± 1.88	9.25 ± 2.84	11.27 ± 1.70
h1 (m)	10	1 – 20	10.1 ± 0.09	10.15 ± 0.82	9.74 ± 0.56	10 ± 0.04	9.85 ± 0.33	9.72 ± 0.18	10 ± 0.02
h2 (m)	250	100 – 500	245 ± 4.9	314.70 ± 61.46	299.55 ± 54.63	247.59 ± 9.84	312.61 ± 26.91	293.21 ± 23.57	247.51 ± 3.93

359

360 **Table 2.** Correlation matrix using 68.27% PDF limit for three layer synthetic resistivity
 361 sounding data.

Model Parameter	ρ_1 (Ωm)	ρ_2 (Ωm)	ρ_3 (Ωm)	h1 (m)	h2 (m)
ρ_1 (Ωm)	1.0000	-0.0575	0.0142	0.3820	0.0222
ρ_2 (Ωm)		1.0000	0.2585	0.6293	-0.7994
ρ_3 (Ωm)			1.0000	0.0537	-0.7678
h1 (m)				1.0000	-0.4278
h2 (m)					1.0000

362

363

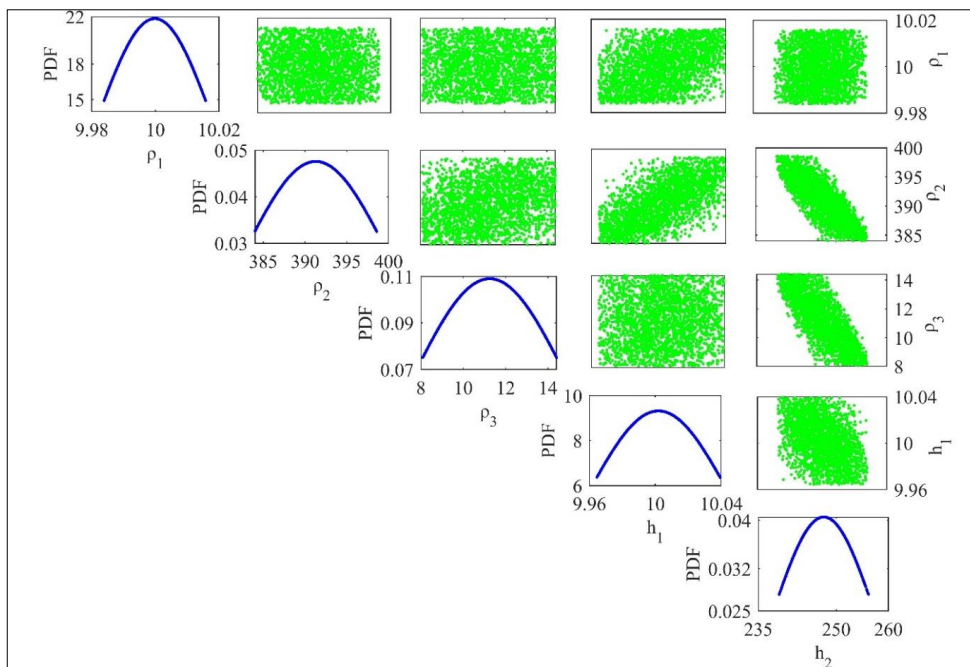
364

365



366 Here, two approaches are used to present the mean solution with its uncertainty
 367 estimation: (i) the mean solution for all accepted best-fitted solutions obtained from 10,000
 368 runs for all three algorithms; and (ii) the mean model calculated from solution with
 369 posterior PDF, which values are greater than 68.27% CI from all accepted solution
 370 parameters.

371 Here, we observed that the second layer parameters for PSO and GWO are too
 372 diverted from actual values with higher uncertainty due to their inability to balance
 373 exploitation and exploration properties. In contrast, the hybrid vPSOGWO algorithm
 374 provides more accurate results and falls within its uncertainty ranges (*Table 1*). Therefore,
 375 a hybrid algorithm has better exploitation and exploration balancing nature than PSO and
 376 GWO. As shown in *Table 2*, the posterior correlation matrix illustrations that first layer
 377 resistivity reveals a feeble correlation with other associated parameters. Whereas there is a
 378 negative correlation found between ρ_2 and h_2 , both parameters have a trade-off
 379 relationship.



380



381 **Figure 6.** Correlation plot between model parameters (off diagonal) and posterior PDF
 382 curve (diagonal) from models having all parameters greater than 68.27% PDF.

383

384 In contrast, a positive correlation between ρ_2 and h_1 is observed (i.e., resistivity of
 385 the second layer increases with increasing the thickness of the first layer and vice versa).
 386 Similarly, it can also be seen between third layer resistivity and second layer thickness but
 387 inverse in nature. *Fig. 6* represents the correlation plot between model parameters (off-
 388 diagonal) with the posterior PDF curve (diagonal) for models greater than 68.27% CI for
 389 all parameters. No significant error differences are found between the observed and
 390 calculated apparent resistivity data for all three algorithms (*Fig. 2(a)*). However, the error
 391 difference in the 1D model and result for 68.27% CI's mean model are presented in *Fig.*
 392 *2(b) and Table 1*, respectively.

393 **Table 3.** Stability test for three layer synthetic resistivity sounding data using different
 394 search range.

Model Parameter	ρ_1 (Ωm)	ρ_2 (Ωm)	ρ_3 (Ωm)	h1 (m)	h2 (m)
True values	10	390	10	10	250
Search Range	5 – 30	500 – 1000	15 – 30	1 – 10	50 – 90
vPSOGWO	10 ± 0.02	390.44 ± 8	10.48 ± 3.60	10 ± 0.04	249.25 ± 9.93
Search Range	2.5 - 30	7.5 – 750	0.1 – 40	1 – 40	50 - 750
vPSOGWO	10 ± 0.03	398.39 ± 18.01	15.93 ± 8.47	10.02 ± 0.07	237.24 ± 21.98
Search Range	1 - 60	1 – 1000	0.01 – 80	1 - 80	1 - 1000
vPSOGWO	10 ± 0.03	428.11 ± 60.40	23.14 ± 13.19	10.10 ± 0.15	214.86 ± 39.66

395

396 To check the stability of the parameter, the hybrid algorithm is tested with three
 397 different search spaces, as shown in *Table 3*. Consequently, it estimates the mean model



398 and uncertainty for 100 runs. This Table illuminates using a broader search space suggests
 399 that the result does not divert too much from the actual model. The computations time
 400 required for vPSOGWO, GWO, and PSO are 1.54s, 1.49s, and 1.48s, respectively, for one
 401 run with 30 data points in this example.
 402 **Table 4.** Optimization mean model result for three layer synthetic resistivity sounding data
 403 with 10% noise.

Model Parameter	True value	Search Range	Mean model (final 10000 solution)			Mean model (PDF > 68.27%)		
			GWO	PSO	vPSOGWO	GWO	PSO	vPSOGWO
ρ_1 (Ωm)	10	5 – 15	10.37 ± 0.56	10.05 ± 0.40	10.04 ± 0.02	10.21 ± 0.24	10.03 ± 0.08	10.04 ± 0.01
ρ_2 (Ωm)	390	15 – 500	323.27 ± 55.51	341.58 ± 49.74	384.37 ± 7.78	317.68 ± 24.39	339.42 ± 23	384.24 ± 3.41
ρ_3 (Ωm)	10	1 – 20	10.46 ± 3.79	9.57 ± 7.78	11.17 ± 3.60	10.61 ± 1.94	9.35 ± 2.84	11.17 ± 1.65
h1 (m)	10	1 – 20	10.16 ± 0.83	9.75 ± 0.57	9.99 ± 0.04	9.89 ± 0.35	9.74 ± 0.18	9.99 ± 0.02
h2 (m)	250	100 – 500	314.65 ± 60.48	300 ± 54.45	251.72 ± 9.59	312.96 ± 27.59	293.61 ± 23.54	251.64 ± 3.82

404
 405 The proposed optimization is also performed using the same synthetic data with
 406 10% Gaussian noise and keeping the search range (*Table 1*). The same procedure is applied
 407 to determine the mean model from all best-fitted solutions and solutions with posterior
 408 PDF greater than 68.27% CI used for parameters of all the solutions (*Table 4*). Although a
 409 10% noise is added, the result obtained from the mean model for posterior PDF of 68.27%
 410 for the hybrid algorithm is not much diverted from actual values. At the same time, the
 411 error was observed that slightly increase $1.309\text{e-}5$, $1.313\text{e-}5$, and $1.327\text{e-}5$ for
 412 vPSOGWO, GWO, and PSO, respectively. *Table 5* depicts the correlation matrix of the
 413 vPSOGWO, which clearly described interdependence by 0.3315 and -0.7879 for the first



414 and second layer's parameters. Similarly, we can also determine the relation between
 415 second layer resistivity and first layer thickness (0.6142), third layer resistivity, and the
 416 second layer thickness (-0.7618). Hence, it shows good agreement with the actual model
 417 values.

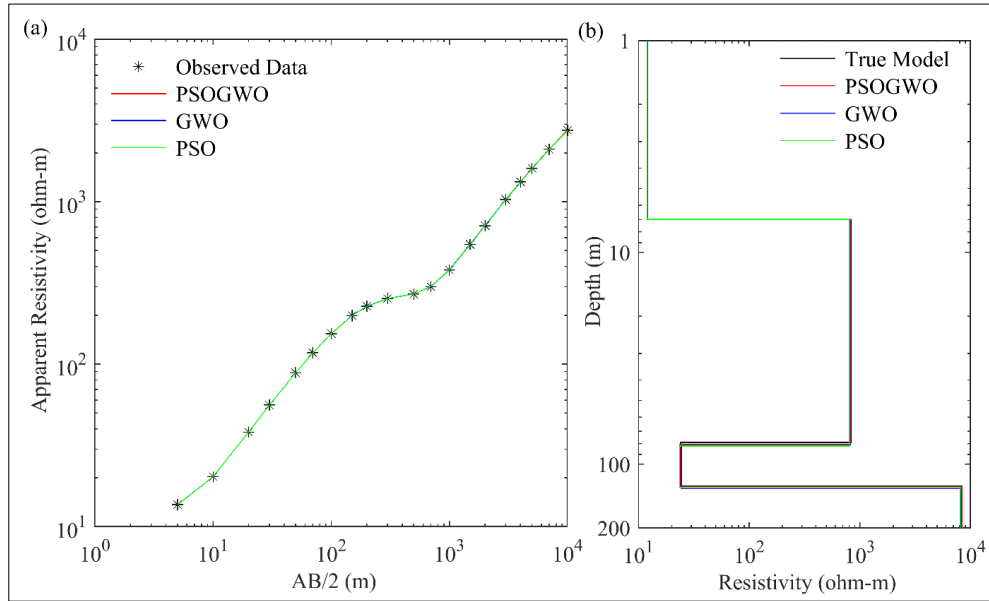
418 **Table 5.** Correlation matrix using 68.27% PDF limit for three layer synthetic resistivity
 419 sounding data with 10% noise.

Model Parameter	ρ_1 (Ωm)	ρ_2 (Ωm)	ρ_3 (Ωm)	h1 (m)	h2 (m)
ρ_1 (Ωm)	1.0000	-0.0816	-0.0017	0.3315	-0.0552
ρ_2 (Ωm)		1.0000	0.2356	0.6142	-0.7879
ρ_3 (Ωm)			1.0000	0.0064	-0.7618
h1 (m)				1.0000	-0.3922
h2 (m)					1.0000

426

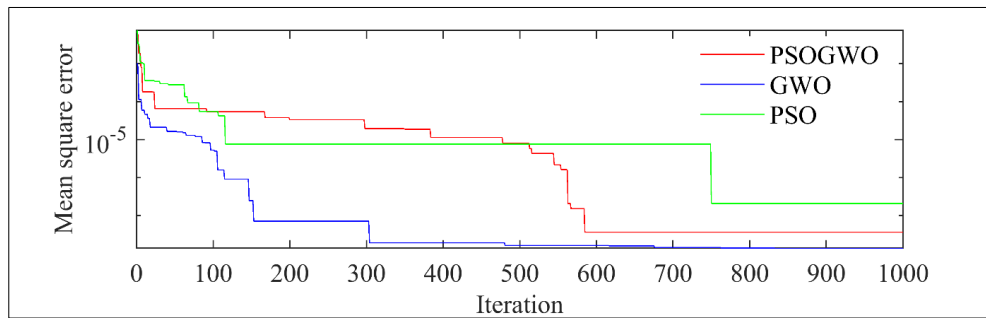
427 6.2 Example 2: Synthetic data- Four layers case

428 The four-layer earth model having a thin, relatively low resistive (24.0 Ωm) sandwiched
 429 between the two high resistivity layers (840.0 Ωm and 8400.0 Ωm) is considered for
 430 demonstration of the proposed algorithms. *Table 6* illustrates the actual model for synthetic
 431 data, search range, and inverted results. The vPSOGWO, GWO, and PSO converge at
 432 iterations 590, 674, and 750 with associated errors 3.624e-8, 1.370e-8, and 2.097e-7,
 433 respectively as shown in *Fig. 8*, whereas the error estimated using ridge regression method
 434 is 0.383. Instead of higher error in vPSOGWO than GWO, it can also be observed that the
 435 error scale for the vPSOGWO algorithm is narrower than the other two algorithms, which
 436 is an essential factor for determining the mean model (*Fig. 9*). Hence, the mean model is
 437 affected by the error scale, as shown in *Fig. 9*.



438

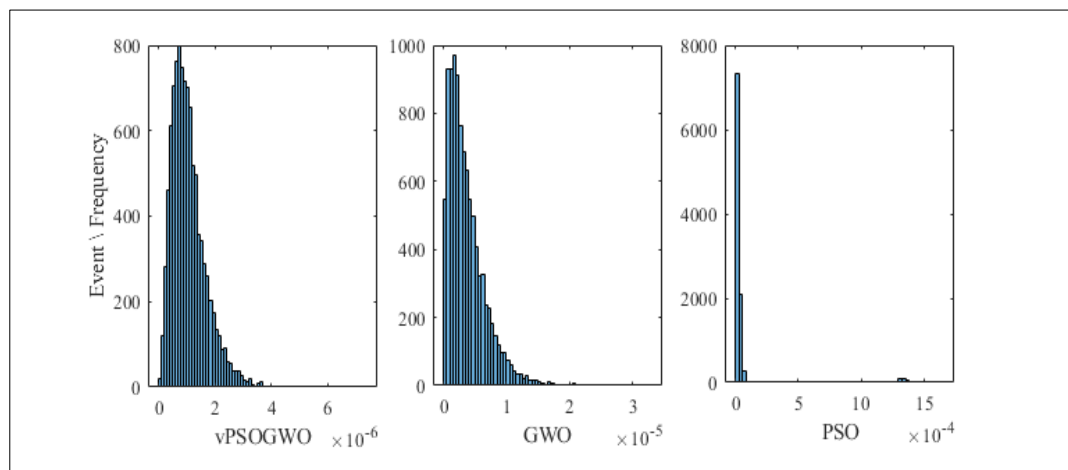
439 **Figure 7.** Four layer synthetic data: (a) observed (*) and the best fitted calculated apparent
440 resistivity curve (> 68.27% PDF); (b) one dimensional mean model (> 68.27% PDF) for
441 true model (black colour), vPSOGWO (red colour), GWO (blue colour) and PSO (green
442 colour).



443

444 **Figure 8.** Convergent curve known as error versus iteration curve for four layers noiseless
445 synthetic resistivity sounding data.

446



447

448 **Figure 9.** Histogram of logarithmic mean square error for vPSOGWO, GWO and PSO

449 over 10,000 models. The x axis of three histogram represent the misfit error correspond to

450 10,000 models.

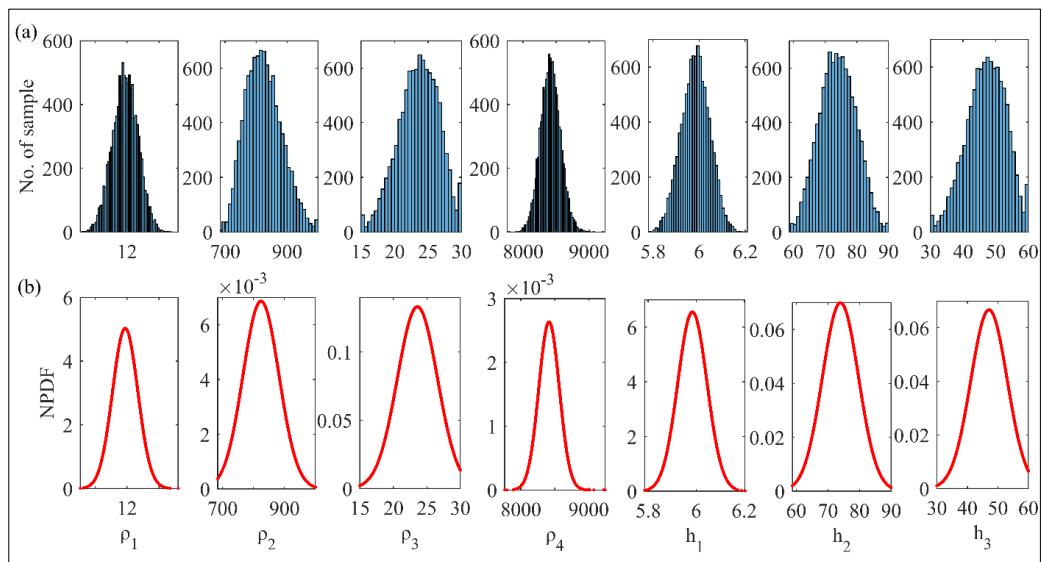
451 **Table 6.** Optimization mean model result for four layer synthetic resistivity sounding data.

Model Parameter	True value	Search Range	Ridge regression	Mean model (final 10000 solution)			Mean model (PDF > 68.27%)		
				GWO	PSO	vPSOGWO	GWO	PSO	vPSOGWO
ρ_1 (Ωm)	12	5 – 30	12.1 ± 0.1	12.03 ± 0.07	12.10 ± 1.05	11.99 ± 0.08	12.02 ± 0.03	12.01 ± 0.39	11.99 ± 0.04
ρ_2 (Ωm)	840	500 – 1000	814 ± 62	809.16 ± 28.80	802.90 ± 69.13	824.36 ± 58.13	814.38 ± 10.86	803.12 ± 31.07	822.71 ± 26.06
ρ_3 (Ωm)	24	15 – 30	18.2 ± 805	24.34 ± 1.30	23.78 ± 5.01	23.59 ± 3	24.50 ± 0.36	23.50 ± 1.95	23.69 ± 1.41
ρ_4 (Ωm)	8400	5000 – 10000	7500 ± 3275	8151.4 ± 293.68	8068.1 ± 614.66	8415.50 ± 151.53	8150.1 ± 118.05	8065.2 ± 301.79	8411.9 ± 70.40
h1 (m)	6	1 – 10	6 ± 0.07	6 ± 0.06	6.04 ± 0.68	5.99 ± 0.06	6 ± 0.03	5.99 ± 0.22	5.99 ± 0.03
h2 (m)	72	50 – 90	74 ± 25.7	75.13 ± 2.82	75.79 ± 7.36	73.99 ± 5.71	74.61 ± 0.94	75.14 ± 3.20	73.77 ± 2.59
h3 (m)	48	30 – 60	36 ± 1595	48.43 ± 2.71	46.98 ± 9.93	47.10 ± 5.98	48.82 ± 0.88	46.46 ± 3.86	47.30 ± 2.81

452



453 To reduce uncertainty and increase the resolution of the model, model parameters
 454 containing posterior PDF greater than 68.27% CI are selected. In *Table 6*, the true model
 455 lies within the uncertainty range of hybrid vPSOGWO, whereas GWO and PSO have failed
 456 to keep the true model within its uncertainty range in the second, third, and fourth layer's
 457 parameters. In the case of ridge regression, the uncertainty level of the model parameters is
 458 too high. For example, in the case of the third layer, both resistivity and thickness have
 459 uncertainty approx. 44 times higher than the actual value.

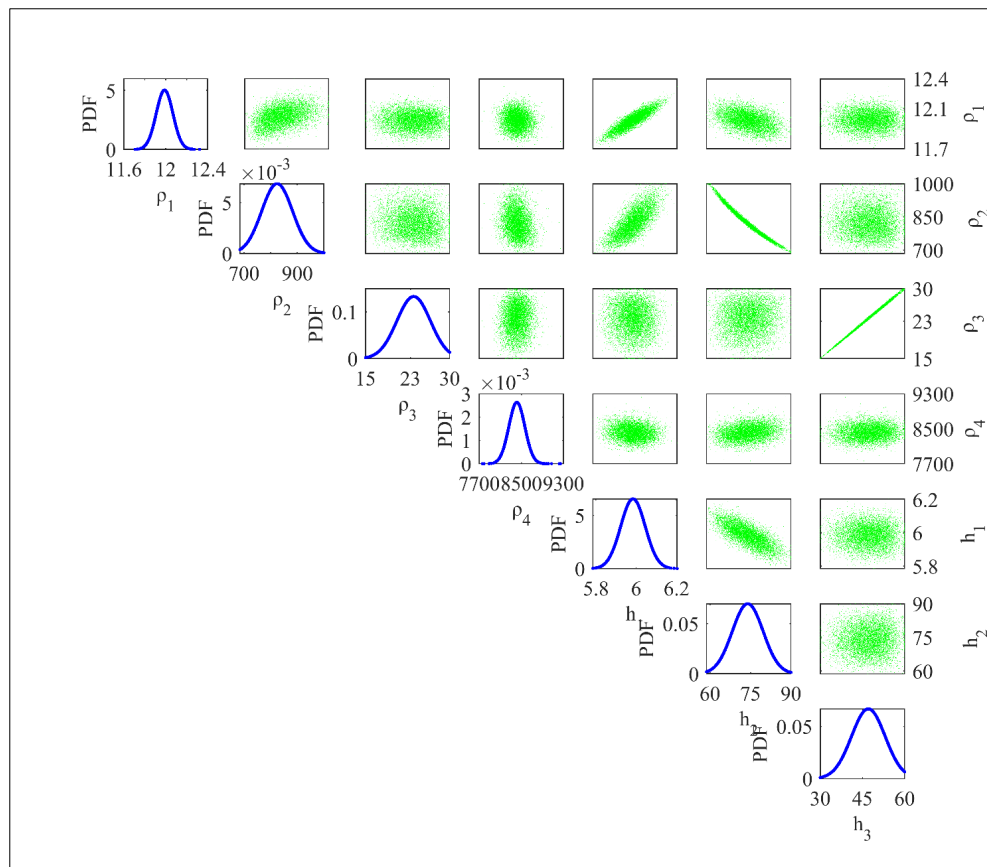


460
 461 **Figure 10.** (a) Histogram and (b) posterior PDF of all 10,000 solution corresponding to
 462 output of each run for four layer synthetic resistivity sounding data.

463
 464 The inverted 10,000 models are also computed in this example to find out the
 465 posterior PDF and histogram for each parameter. The peak of posterior PDF is roughly
 466 nearby the actual solution, as shown in histogram *Fig. 10(a) and Fig. 10(b) reveals the ρ_2*
 467 *and h_2 have a broader range that signifies the equivalence problem associated with the*
 468 *resistive layer. The uncertainty in each algorithm is found to be large considering all the*



469 accepted models. However, picking the models with greater posterior PDF than 68.27% CI
 470 reduces the uncertainty in the model, increases the resolution of a solution.



471

472 **Figure 11.** Correlation plot between model parameters (off diagonal) and posterior PDF
 473 curve (diagonal) from models having all parameters greater than 68.27% PDF.

474

475 The correlation plot between model parameters (off-diagonal) with the posterior
 476 PDF curve (diagonal) for models greater than 68.27% CI for all parameters is shown in
 477 Fig. 11. There are also no significant error differences between the computed and observed
 478 apparent resistivity data for all three optimization algorithms.



479 **Table 7.** Correlation matrix using 68.27% PDF limit for four layer synthetic resistivity
 480 sounding data.

Model Parameter	ρ_1 (Ωm)	ρ_2 (Ωm)	ρ_3 (Ωm)	ρ_4 (Ωm)	h1 (m)	h2 (m)	h3 (m)
ρ_1 (Ωm)	1.0000	-0.0359	-0.0029	-0.0207	0.7383	0.0354	-0.0041
ρ_2 (Ωm)		1.0000	-0.0481	-0.0598	0.4667	-0.9798	-0.0105
ρ_3 (Ωm)			1.0000	0.0284	-0.0188	0.0274	0.9983
ρ_4 (Ωm)				1.0000	-0.0183	0.0935	0.0509
h1 (m)					1.0000	-0.4286	-0.0036
h2 (m)						1.0000	-0.0079
h3 (m)							1.0000

481

482 The correlation matrix of a four-layer model of synthetic resistivity data is shown in
 483 *Table 7*. It illustrates that the first layer parameters are correlated by a correlation matrix
 484 of 0.7383. A strong negative correlation was found between the second layer parameters (-
 485 0.9798), and the third layer parameters are strongly correlated with each other by a positive
 486 correlation matrix of 0.9983. *Fig. 7(a)* shows the fitness between four-layer synthetic (*)
 487 and computed apparent resistivity data obtained for vPSOGWO, GWO, and PSO. The
 488 difference in fitness curves for all three optimization techniques cannot be determined as
 489 the observed error is significantly negligible. However, the error difference can be
 490 observed in the 1D resistivity-depth models obtained from 68.27% CI's mean model, as
 491 shown in *Fig. 7(b)*. *Table 6* shows the mean model having posterior PDF greater than
 492 68.27% CI for all accepted parameters in the four-layer earth model case. The computation
 493 time for vPSOGWO, GWO, and PSO are 1.94s, 1.84s, and 1.85s (PSO), respectively, for
 494 one run with 27 data points in this example.

495 The optimization techniques are also executed using the same four-layer model of
 496 synthetic data with 10% Gaussian noise and keeping the search range in *Table 6*. The



497 same procedure is applied to determine the mean model from all the best-fitted models
 498 and models of a posterior PDF greater than 68.27% CI for all model parameters
 499 presented in *Table 8*. Although a 10% noise is added, the result obtained from the mean
 500 model for the posterior PDF of 68.27% for the hybrid algorithm is not much diverted
 501 from actual values. At the same time, the experimental error is $3.831e-4$, $3.831e-4$, and
 502 $3.870e-4$ for vPSOGWO, GWO, and PSO, respectively.

503 **Table 8.** Optimization mean model result for four layer synthetic resistivity sounding
 504 data with 10% noise.

Model Parameter	True value	Search Range	Mean model (final 10000 solution)			Mean model (PDF > 68.27%)		
			GWO	PSO	vPSOGWO	GWO	PSO	vPSOGWO
ρ_1 (Ωm)	12	5 - 30	12.25 ± 0.07	12.38 ± 1.03	12.27 ± 0.09	12.24 ± 0.03	12.26 ± 0.37	12.27 ± 0.04
ρ_2 (Ωm)	840	500 – 1000	813.70 ± 31.51	816.76 ± 66.79	901.03 ± 53.95	812.08 ± 12.36	816.46 ± 29.21	899.24 ± 24.66
ρ_3 (Ωm)	24	15 - 30	24.17 ± 1.36	23.51 ± 5.03	23.59 ± 2.84	24.31 ± 0.42	23.28 ± 1.87	23.50 ± 1.37
ρ_4 (Ωm)	8400	5000 - 10000	8070.5 ± 310.96	7971.2 ± 596.07	8415.50 ± 167.11	8082 ± 143.09	7973.5 ± 292.28	8417 ± 80.27
h1 (m)	6	1 - 10	6.15 ± 0.06	6.22 ± 0.67	5.99 ± 0.06	6.15 ± 0.03	6.15 ± 0.21	6.20 ± 0.03
h2 (m)	72	50 - 90	76.80 ± 2.98	76.96 ± 6.96	73.99 ± 4.59	76.72 ± 1.29	76.38 ± 3.00	69.75 ± 2.10
h3 (m)	48	30 - 60	47.35 ± 2.84	47.35 ± 10.09	47.10 ± 5.85	48.75 ± 0.94	47.02 ± 3.77	48.27 ± 2.83

505
 506 *Table 9* illustrates the correlation matrix of the hybrid algorithm, which clearly
 507 described interdependence by 0.7644, -0.9665 , and 0.9980 for the first and second, and
 508 third layers parameters. Similarly, we can also find out the relation between second layer
 509 resistivity and first layer thickness (0.3605) and the resistivity of the fourth layer and



510 thickness of the third layer (0.0549). Hence, it shows good agreement with the actual
 511 model values.

512 **Table 9.** Correlation matrix using 68.27% PDF limit for four layer synthetic resistivity
 513 sounding data with 10% noise.

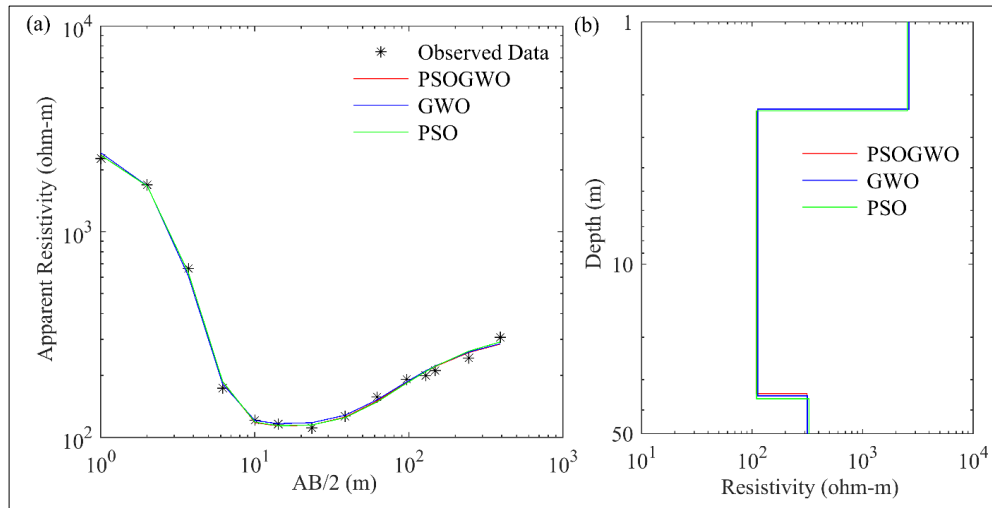
Model Parameter	ρ_1 (Ωm)	ρ_2 (Ωm)	ρ_3 (Ωm)	ρ_4 (Ωm)	h1 (m)	h2 (m)	h3 (m)
ρ_1 (Ωm)	1.0000	0.0003	0.0271	-0.0948	0.7644	-0.0109	0.0251
ρ_2 (Ωm)		1.0000	-0.0168	0.0327	0.3605	-0.9665	0.0153
ρ_3 (Ωm)			1.0000	0.0260	0.0211	-0.0042	0.9980
ρ_4 (Ωm)				1.0000	-0.0446	0.0009	0.0549
h1 (m)					1.0000	-0.3180	0.0268
h2 (m)						1.0000	-0.0329
h3 (m)							1.0000

514

515

516 **6.3 Example 3: Field data - Three-layer case**

517 We have taken one three-layer case of vertical electrical resistivity sounding data measured
 518 with Schlumberger array over Mt. Turner, North Queensland, Australia, interpreted by
 519 Dixon and Doherty (1977, *Fig. 2a*), as shown in *Fig. 12(a)*. After selecting a suitable
 520 search range, three novel algorithms, namely vPSOGWO, GWO, and PSO, are executed to
 521 reconstruct the model interpreted by Dixon and Doherty (1977). The search range and
 522 comparison among proposed algorithms with the previous result (Dixon and Doherty,
 523 1977) are presented in *Table 10*. Our results (for 68.27% CI) are closed to the development
 524 given by Dixon and Doherty (1977). The convergent error for the best-fitted model in
 525 vPSOGWO is $3.681\text{e-}4$, whereas GWO is $3.697\text{e-}4$, and PSO is $3.682\text{e-}4$.



526

527 **Figure 12.** Three layer field data over Mt. Turner, North Queensland, Australia: (a)
 528 observed (*) and the best fitted calculated apparent resistivity curve (> 68.27% PDF); (b)
 529 one dimensional mean model (> 68.27% PDF) for true model (black colour), vPSOGWO
 530 (red colour), GWO (blue colour) and PSO (green colour).

531 **Table 10.** Optimization mean model result for three layer field resistivity sounding data.

Model Parameter	Search Range	Dixon and Doherty (1977)	Mean model (final 10000 solution)			Mean model (PDF > 68.27%)		
			GWO	PSO	vPSOGWO	GWO	PSO	vPSOGWO
ρ_1 (Ωm)	2000 – 3000	2500	2646.6 ± 246.65	2532.3 ± 78.20	2536 ± 8.67	2619.8 ± 109.70	2533.8 ± 34.59	2535.9 ± 4.05
ρ_2 (Ωm)	10 – 400	100	116.01 ± 16.45	110.17 ± 3.38	109.23 ± 0.29	112.55 ± 4.65	109.78 ± 1.11	109.24 ± 0.13
ρ_3 (Ωm)	200 – 500	300	318.99 ± 31.67	334.01 ± 33.22	314.42 ± 1.63	315.50 ± 11.96	327.15 ± 14.93	314.40 ± 0.77
h1 (m)	0.1 – 3	1.42 (approx.)	1.28 ± 0.13	1.33 ± 0.02	1.33 ± 0.00	1.29 ± 0.05	1.33 ± 0.01	1.33 ± 0.00
h2 (m)	20 - 50	29.21 (approx.)	34.02 ± 7.38	34.91 ± 6.29	31.90 ± 0.31	32.66 ± 2.99	33.67 ± 2.17	31.90 ± 2.17

532

533



534 **Table 11.** Correlation matrix using 68.27% PDF limit for three layer field resistivity
 535 sounding data.

Model Parameter	ρ_1 (Ωm)	ρ_2 (Ωm)	ρ_3 (Ωm)	h1 (m)	h2 (m)
ρ_1 (Ωm)	1.0000	0.0046	-0.0003	-0.2336	0.0086
ρ_2 (Ωm)		1.0000	-0.0389	-0.0897	0.3075
ρ_3 (Ωm)			1.0000	0.0144	0.4050
h1 (m)				1.0000	-0.0256
h2 (m)					1.0000

536

537 *Table 11* presents the correlation matrix, which shows a negative correlation
 538 between the first layer parameters, and a positive correlation is observed between the
 539 second layer parameters. A positive correlation is also observed between ρ_3 and h_2 , which
 540 maintains the same model data. *Fig. 12(a)* shows the apparent resistivity curve and the 1D
 541 model obtained from the mean model with a 68.27% CI result shown in *Fig. 12(b)*. The
 542 computation time requires for one run in this example with 14 data points is 0.90s
 543 (vPSOGWO), 0.83s (GWO), and 0.78s (PSO), respectively.

544

545 **6.4 Example 4: Field data - Five-layer case**

546 We have selected another field example using a vertical electrical resistivity sounding data
 547 as a five-layer case of earth's subsurface model from Keshiari-Kharagpur near Kharagpur,
 548 West Bengal, India, to determine the aquifer zone (Panda et al., 2018, *Fig. 3*). The area is
 549 covered with different geological units such as laterite, clay, sand, etc., and laterite material
 550 restricts the aquifer's recharge process and most problematic area for groundwater
 551 potential. We inverted this data for a five-layered earth structure parameter using the
 552 vPSOGWO, GWO, and PSO inversion algorithm. The results are shown in *Table 12*
 553 available model, borehole sample, and the search space for vPSOGWO, GWO, and PSO.



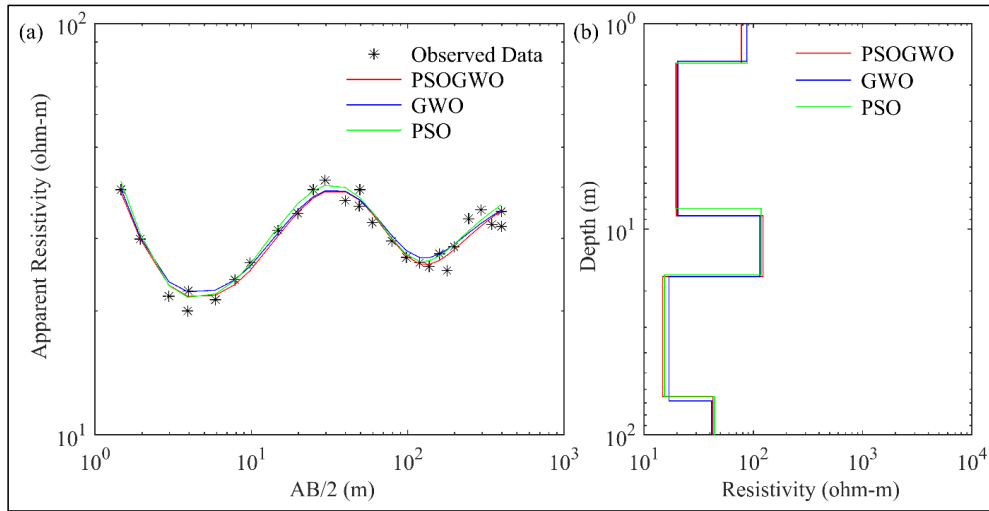
554 The computed apparent resistivity curve for all the three algorithms (-) and field data
 555 indicated by the symbol (*) are shown in *Fig. 13(a)*. Their error differences are significant
 556 (*Fig. 13a, Table 12*). The inverted 1D layered model using all algorithms obtained from
 557 68.27% CI's mean model is shown in *Fig. 13(b)*. The computations time for vPSOGWO,
 558 GWO, and PSO are 2.55s, 2.43s, and 2.45s, respectively, for one run with 28 data points in
 559 this example.

560 **Table 12.** Optimization mean model result for five layer field resistivity sounding data.

Model Parameter	Search Range	Litho log detail of 100m deep	VES6 (Panda et al., 2017) VFSA	Mean model (final 10000 solution)			Mean model (PDF > 68.27%)		
				GWO	PSO	vPSOGWO	GWO	PSO	vPSOGWO
ρ_1 (Ωm)	60 – 120	--	97 ± 5	87.97 ± 10.02	88.41 ± 13.73	78.21 ± 8.28	87.44 ± 3.37	88.43 ± 5.31	77.99 ± 3.17
ρ_2 (Ωm)	10 – 30	--	19 ± 0.2	20.38 ± 0.87	19.38 ± 1.18	19.73 ± 0.17	20.43 ± 0.34	19.43 ± 0.43	19.73 ± 0.06
ρ_3 (Ωm)	80 – 150	--	128 ± 29	116.04 ± 10.01	118.34 ± 14.41	123.24 ± 9.56	115.28 ± 3.50	117.55 ± 5.67	123.01 ± 3.67
ρ_4 (Ωm)	10 – 25	--	60 ± 1	16.79 ± 1.31	15.27 ± 2.12	14.83 ± 0.69	16.93 ± 6.49	15.35 ± 0.83	14.84 ± 0.27
ρ_5 (Ωm)	25 – 60	--	40 ± 0.4	41.91 ± 2.99	44.46 ± 3.60	42.83 ± 0.52	41.61 ± 1.06	44.28 ± 1.35	42.67 ± 0.20
h1 (m)	0.2 – 0.9	0.6 (Dry soil)	0.5 ± 0.1	0.54 ± 0.05	0.56 ± 0.06	0.56 ± 0.02	0.53 ± 0.02	0.56 ± 0.02	0.56 ± 0.01
h2 (m)	5 – 10	7 (Moist soil)	6.5 ± 0.3	7.06 ± 0.56	6.35 ± 1.01	7.06 ± 0.13	7.10 ± 0.21	6.36 ± 0.35	7.06 ± 0.05
h3 (m)	6 – 10	8 (Compact laterite)	7.7 ± 2.3	8.41 ± 0.72	8.78 ± 1.33	8.37 ± 0.68	8.38 ± 0.26	8.77 ± 0.53	8.37 ± 0.26
h4 (m)	40 – 55	48 (Soft laterite)	45.0 ± 5.0	51.15 ± 3.57	48.34 ± 6.10	48.22 ± 3.28	51.37 ± 1.37	48.60 ± 2.42	48.23 ± 1.27

561

562 * The symbol “- -” in table stand for no information.



563

564 **Figure 13.** Five layer field data: (a) observed (*) and the best fitted calculated apparent
 565 resistivity curve (> 68.27% PDF); (b) one dimensional mean model (> 68.27% PDF) for
 566 true model (black colour), vPSOGWO (red colour), GWO (blue colour) and PSO (green
 567 colour).

568 **Table 13.** Correlation matrix using 68.27% PDF limit for five layer field resistivity
 569 sounding data.

Model Parameter	ρ_1 (Ωm)	ρ_2 (Ωm)	ρ_3 (Ωm)	ρ_4 (Ωm)	ρ_5 (Ωm)	h1 (m)	h2 (m)	h3 (m)	h4 (m)
ρ_1 (Ωm)	1.0000	0.8103	0.0246	0.0164	0.1051	-0.9779	0.5888	-0.0288	0.0492
ρ_2 (Ωm)		1.0000	0.1267	-0.1124	0.0684	-0.8652	0.7855	-0.1035	-0.0675
ρ_3 (Ωm)			1.0000	-0.1272	-0.1221	-0.0390	0.6185	-0.9664	-0.1169
ρ_4 (Ωm)				1.0000	0.4706	0.0028	-0.3107	-0.0985	0.9726
ρ_5 (Ωm)					1.0000	-0.1026	-0.0414	0.0449	0.6416
h1 (m)						1.0000	-0.6356	0.0392	-0.0328
h2 (m)							1.0000	-0.5463	-0.2534
h3 (m)								1.0000	-0.0936
h4 (m)									1.0000

570



571 The result obtained from the mean solution of all accepted solutions and solutions
572 with PDF greater than 68.27% CI aimed at all parameters using the developed techniques
573 is presented in *Table 12*. The final mean models are comparable with lithological data of
574 100m deep tube well near VES6. The convergent error for vPSOGWO, GWO, and PSO
575 are $4.498e-4$, $4.541e-4$, and $4.566e-4$, respectively, whereas the error is $1.7e-2$ for VFSA
576 obtained by Panda et al. (2018). The correlation matrix clarifies a strong correlation
577 between the parameters of the first layer (-0.9736), the second layer (0.8434), and the third
578 layer (-0.9907) and a moderate relation between the parameters of the fourth layer
579 (0.5653). We have noticed a moderate interdependence between ρ_3 with h_2 and ρ_5 with h_4 ,
580 which follows to retain the same model data shown in *Table 13*.

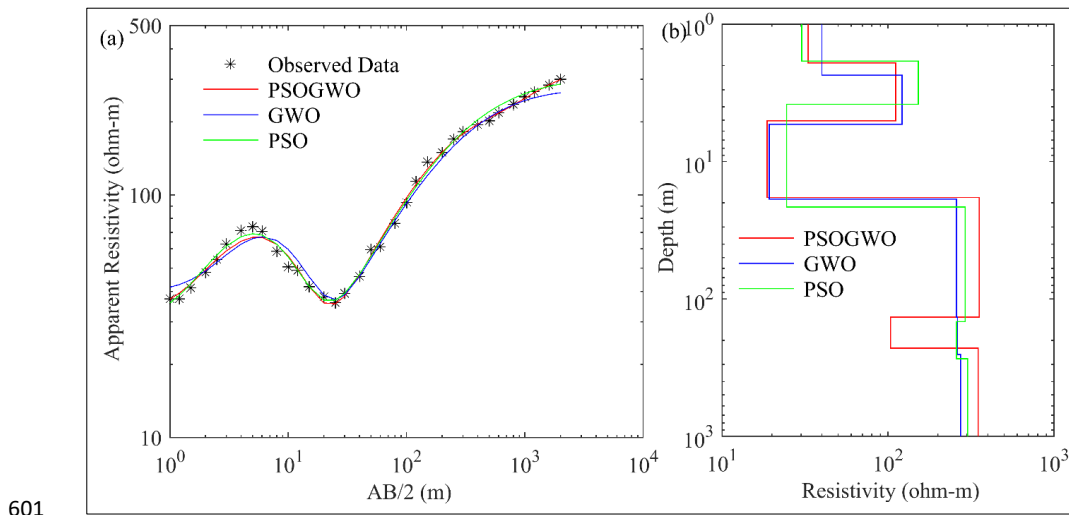
581

582 **6.5 Example 5: Field data - Six layer case**

583 We again applied the vPSOGWO, GWO, and PSO algorithms to invert the field apparent
584 resistivity data as a six-layer case study extracted near a borehole from in Apulia, South Italy,
585 for hydrogeological purposes (Sen et al. 1993). The search range has been taken from Sen et
586 al. (1993), but the fourth and upper bound thickness of the fifth layers increases by 50 m, as
587 shown in *Table 14*. The reproduced field data (*) and inverted field data (-) are shown in *Fig.*
588 *14(a)*. The misfit error obtained is $2.830e-4$, $3.243e-4$, and $3.133e-4$ for vPSOGWO, GWO,
589 and PSO, respectively, whereas the error using Simulating Annealing (SA) is 0.017 by Sen et
590 al. (1993). *Table 14* also includes the mean model for 100% and 68.27% CI using proposed
591 algorithms and previously published literature. It is observed that few parameters obtained
592 fall within the uncertainty of corresponding parameters of vPSOGWO. The vPSOGWO
593 inverted results provide higher similarity with the borehole information than the results by
594 SA (Sen et al., 1993). The interdependence between the layer parameter can be seen from the
595 correlation matrix as shown in *Table 15*. A strong correlation among parameters of the first



596 layer (0.8211), the second layer (−0.9327), and the third layer (0.9766) has been shown by the
597 correlation matrix, which is comparable to the correlation matrix that has been presented by
598 Sen et al. (1933 *Table 13*). A moderate correlation between fourth (−0.5246) and fifth layer
599 parameters (0.4486) is also observed. It is also to be noticed that there is a sensible relation
600 between sixth layer resistivity and fifth layer thickness, keeping the same model data.



601
602 **Figure 14.** Six layer field data over Keshiari-Kharagpur near Kharagpur, India: (a)
603 observed (*) and the best fitted calculated apparent resistivity curve (> 68.27% PDF); (b)
604 one dimensional mean model (> 68.27% PDF) for true model (black colour), vPSOGWO
605 (red colour), GWO (blue colour) and PSO (green colour).

606 The error differences in computed data with observed data are significant, as shown
607 in *Fig. 14(a)* and *Table 12*. The inverted 1D layered models obtained from the mean model
608 of 68.27% CI are shown in *Fig. 14(b)*. The computations time for vPSOGWO, GWO, and
609 PSO are 3.58s, 3.44s, and 3.45s, respectively, for one run with 28 data points in this
610 example. The inverted results from vPSOGWO, GWO, and PSO have been shown along
611 with the borehole data, published result (Sen et al., 1993) in *Table 14*. It can note that the



612 outcomes from the hybrid algorithm satisfy the borehole information provided than the

613 other algorithms and earlier published results.

614 **Table 14.** Optimization mean model result for six layer field resistivity sounding data.

Model Parameter	Search Range	Borehole Detail from Patella, 1975	Sen et al., 1993		Mean model (final 10000 solution)			Mean model (PDF > 68.27%)		
					GWO	PSO	vPSOGWO	GWO	PSO	vPSOGWO
ρ_1 (Ωm)	10 - 50	--	37	33 ± 4.91	36.47 ± 6.23	30.00 ± 8.49	32.93 ± 1.60	40 ± 2.41	30.24 ± 2.08	33.06 ± 0.57
ρ_2 (Ωm)	50 - 250	--	140	240 ± 29.63	121.81 ± 29.04	158.49 ± 49.17	112.32 ± 24.59	121.42 ± 11.63	152.01 ± 20.51	111.25 ± 9.33
ρ_3 (Ωm)	1 - 40	--	17	24 ± 1.37	19.38 ± 4.58	24.14 ± 7.07	18.19 ± 3.21	19.26 ± 1.85	24.49 ± 2.08	18.70 ± 1.15
ρ_4 (Ωm)	100 - 600	--	340	300 ± 17.5	278.55 ± 71.41	299.07 ± 53.73	355.16 ± 42.70	258.02 ± 30.37	291.83 ± 23.55	354.49 ± 16.04
ρ_5 (Ωm)	30 - 500	--	130	120 ± 32.09	276.27 ± 80.72	265.25 ± 65.06	105.80 ± 39.26	262.16 ± 33.24	259.27 ± 30.44	103.67 ± 14.50
ρ_6 (Ωm)	100 - 500	--	300	320 ± 8.33	286.46 ± 46.72	303.76 ± 27.36	349.29 ± 20.98	273.73 ± 21.91	301.75 ± 12.34	349.68 ± 7.90
h1 (m)	0.5 - 3	1 (Aluvial soil)	1.3	1.1 ± 0.198	1.32 ± 0.48	0.96 ± 0.66	0.91 ± 0.09	1.36 ± 0.16	0.86 ± 0.10	0.92 ± 0.03
h2 (m)	1 - 8	3 (Fine sand)	2.7	1.3 ± 0.252	3.17 ± 0.98	2.13 ± 1.16	3.16 ± 0.47	3.01 ± 0.41	1.97 ± 0.34	3.13 ± 0.18
h3 (m)	1 - 25	12.5 (Calcarenit e & sandy clay)	12	17 ± 1.13	13.66 ± 3.49	17.72 ± 6.03	12.93 ± 2.74	13.41 ± 1.36	17.57 ± 1.94	13.26 ± 1.02
h4 (m)	10 - 200	118.5 (Calcareous tufa & limestone)	120	125 ± 8.39	117.93 ± 33.89	124.38 ± 29.15	118.95 ± 30.44	117.28 ± 12.31	125.08 ± 13.71	117.72 ± 11.72
h5 (m)	10 - 200	65 (Water bearing limestone)	120	70 ± 23.15	118.79 ± 34.45	127.62 ± 29.37	93.12 ± 33.99	116.89 ± 12.36	125.98 ± 13.51	92.85 ± 13.03

615



616 **Table 15.** Correlation matrix using 68.27% PDF limit for six layer field resistivity sounding
 617 data.

Model Parameter	ρ_1 (Ωm)	ρ_2 (Ωm)	ρ_3 (Ωm)	ρ_4 (Ωm)	ρ_5 (Ωm)	ρ_6 (Ωm)	h1 (m)	h2 (m)	h3 (m)	h4 (m)	h5 (m)
ρ_1 (Ωm)	1.000	0.478	-0.088	-0.11	0.086	-0.056	0.933	-0.446	-0.087	0.024	0.015
ρ_2 (Ωm)		1.000	0.3732	0.11	-0.077	0.134	0.718	-0.902	0.379	0.068	0.095
ρ_3 (Ωm)			1.000	0.54	-0.388	0.392	0.005	-0.661	0.988	0.021	0.186
ρ_4 (Ωm)				1.00	-0.623	0.487	-0.088	-0.126	0.647	-0.420	0.274
ρ_5 (Ωm)					1.000	-0.668	0.070	0.173	-0.458	-0.109	0.022
ρ_6 (Ωm)						1.000	-0.027	-0.223	0.449	0.324	0.528
h1 (m)							1.000	-0.655	0.006	0.044	0.033
h2 (m)								1.000	-0.655	-0.068	-0.131
h3 (m)									1.000	-0.033	0.217
h4 (m)										1.000	-0.014
h5 (m)											1.000

618

619

620 **7.0 CONCLUSION**

621 We have evaluated three meta-heuristic algorithms such as PSO, GWO, and vPSOGWO to
 622 realize their efficacy and applicability in the geoelectrical inverse problems, which narrates
 623 the appraisal of 1D resistivity models from geoelectrical resistivity sounding data. The
 624 relevance of these algorithms validated using synthetic and field resistivity sounding data
 625 signifying the kinds of earth's subsurface stratigraphy. An enormous solution 569
 626 (100,000,000 from 10,000 runs) is assessed. Subsequently, the best-fitted solutions are
 627 chosen within a pre-distinct value for statistical measurements. The statistical study
 628 includes posterior PDF with 68.27% CI, a mean solution, posterior solution correlation
 629 matrix, and covariance matrix using search space, was carried out to refine the solutions to
 630 obtain the global mean solution with the least uncertainty. These statistical simulations



631 yield essential information as to the reliability of an inversion algorithm. In general,
632 conventional techniques can be quite effective in resolving the model in random noise but
633 can fail in systematic error and inappropriate models. Our investigation with the
634 application of the developed algorithm, including statistical simulation for different
635 multilayer resistivity parameters, resulted in a quantitative appraisal of uncertainty in the
636 derived model parameters. We observed that the output of the hybrid algorithm in terms of
637 mean model or error might be similar to either PSO or GWO (attributed to the exploration
638 characteristics of GWO and exploitation characteristics of PSO). The vPSOGWO, GWO,
639 and PSO algorithms performances have been analyzed based on the uncertainty and
640 stability and mean model of layered earth structure. We found that the vPSOGWO gives
641 very closer results than the results inverted from other two algorithms and also
642 conventional methods which is consistently better than the previously published results,
643 and correlated well with borehole information.

644

645 **CONFLICT OF INTEREST**

646 There are no conflicts of interest declared by the authors.

647

648 **DATA AVAILABILITY STATEMENT**

649 The data the support the findings of this study will be available on the request from
650 corresponding authors. All the data taken for study to demonstrate our developed algorithms
651 are a published/public domain data that obviously written in the manuscript.

652

653 **REFERENCES**

654 Colorni, A., Dorigo, M., Maniezzo, V., 1991. Distributed optimization by ant colonies.
655 In Proceedings of the first European conference on artificial life 142, 134-142.



- 656 Dixon, O., Doherty, J. E., 1977. New interpretation methods for IP soundings. Exploration
657 Geophysics 8, 65-69. <https://doi.org/10.1071/EG977065>.
- 658 Eiben, A. E., Schippers, C. A., 1998. On evolutionary exploration and exploitation.
659 Fundamenta Informaticae 35, 35-50. <https://doi.org/10.3233/FI-1998-35123403>.
- 660 Esmín, A. A., Matwin, S., 2013. HPSOM: a hybrid particle swarm optimization algorithm
661 with genetic mutation. International Journal of Innovative Computing, Information,
662 and Control. 9, 1919-1934.
- 663 Kennedy, J., Eberhart, R., 1995. Particle swarm optimization. In Proceedings of ICNN'95-
664 International Conference on Neural Networks IEEE 4, 1942-1948.
665 <https://doi.org/10.1109/ICNN.1995.488968>.
- 666 Koefoed, O., 1979. Geosounding principles, 1: Resistivity sounding measurements.
667 Methods in Geochemistry and Geophysics: Elsevier Science Ltd. Co., Amsterdam,
668 14A, pp 276.
- 669 Kamboj, V. K., 2015. A novel hybrid PSO–GWO approach for unit commitment Problem.
670 Neural Computing and Applications 27(6), 1643-1655. [https://doi.org/10.1007/s00521-
671 015-1962-4](https://doi.org/10.1007/s00521-015-1962-4).
- 672 Lai, X., Zhang, M., 2009. An efficient ensemble of GA and PSO for real function
673 optimization. In 2009 2nd IEEE International Conference on Computer Science and
674 Information Technology IEEE, 651-655. <https://doi.org/10.1109/ICCIA.2010.6141614>.
- 675 Mirjalili, S., Hashim, S. Z. M., 2010. A new hybrid PSO-GSA algorithm for function
676 optimization. In 2010 International conference on computer and information
677 application IEEE, 374-377. <https://doi.org/10.1109/ICCIA.2010.614161>.
- 678 Mirjalili, S., Mirjalili, S.M., Lewis, A., 2014. Grey wolf optimizer. Advances in
679 engineering software 69, 46-61. <https://doi.org/10.1016/j.advengsoft.2013.12.007>.



- 680 Mosegaard, K., Tarantola, A., 1995. Monte Carlo sampling of solutions to inverse problems.
681 Journal of Geophysical Research Atmospheres 1001, 12431-12448.
682 <https://doi.org/10.1029/94JB03097>.
- 683 Mitchell, M., 1998. An introduction to genetic algorithms. A Bradford Book, The MIT Press.
- 684 Narayan, S., Dusseault, M. B., Nobes, D. C., 1994. Inversion techniques applied to resistivity
685 inverse problems. Inverse Problems 10, 669–686.
- 686 Oldenburg, D. W., Li, Y., 1994. Inversion of induced polarization data. Geophysics 59,
687 1327–1341. <https://doi.org/10.1190/1.1443692>.
- 688 Panda, K. P., Sharma, S. P., Jha, M. K., 2018. Mapping lithological variations in a river
689 basin of West Bengal, India using electrical resistivity survey implications for
690 artificial recharge. Environmental Earth Sciences 77, 1-10.
691 <https://doi.org/10.1007/s12665-018-7813-8>.
- 692 Parasnis D. S., 1980. Principles of Applied Geophysics. Fourth ed., New York, Chapman,
693 and Hall.
- 694 Pekeris, C. L., 1940. Direct method of interpretation in resistivity prospecting. Geophysics
695 5, 31-42. <https://doi.org/10.1190/1.1441791>.
- 696 Rashedi, E., Nezamabadi-Pour, H., Saryazdi, S., 2009. GSA: a gravitational search
697 algorithm. Information sciences 179, 2232-2248.
698 <https://doi.org/10.1016/j.ins.2009.03.004>.
- 699 Roshan, R., Singh, U. K., 2017. Inversion of residual gravity anomalies using tuned PSO.
700 Geoscientific Instrumentation Methods and Data Systems 6, 71-79.
701 <https://doi.org/10.5194/gi-6-71-2017>.
- 702 Ross, S., 2009. Probability and statistics for engineers and scientists. Elsevier, New
703 Delhi, 16, 32-33.



- 704 Sen, M. K., Bhattacharya, B. B., Stoffa, P. L., 1993. Nonlinear inversion of resistivity
705 sounding data. *Geophysics* 58, 496-507. <https://doi.org/10.1190/1.1443432>.
- 706 Şenel, F. A., Gökçe, F., Yüksel, A. S., Yiğit, T., 2019. A novel hybrid PSO–GWO
707 algorithm for optimization problems. *Engineering with Computers* 35, 1359-1373.
708 <https://doi.org/10.1007/s00366-018-0668-5>.
- 709 Singh, N., Singh, S. B., 2017. Hybrid algorithm of particle swarm optimization and grey
710 wolf optimizer for improving convergence performance. *Journal of Applied*
711 *Mathematics*, 1-15. <https://doi.org/10.1155/2017/2030489>.
- 712 Singh, U. K., Tiwari, R.K., Singh, S.B., 2005. One-dimensional inversion of geo-electrical
713 resistivity sounding data using artificial neural networks—a case study. *Computers &*
714 *Geosciences* 31, 99-108. <https://doi.org/10.1016/j.cageo.2004.09.014>.
- 715 Singh, U. K., Tiwari, R.K., Singh, S.B., 2013. Neural network modeling and prediction of
716 resistivity structures using VES Schlumberger data over a geothermal area.
717 *Computers & Geosciences* 52, 246-257. <https://doi.org/10.1016/j.cageo.2012.09.018>.
- 718 Sharma, S. P., 2012. VFSARES—a very fast simulated annealing FORTRAN program for
719 interpretation of 1-D DC resistivity sounding data from various electrode
720 arrays. *Computers & Geosciences* 42, 177-188.
721 <https://doi.org/10.1016/j.cageo.2011.08.029>.
- 722 Simon, D., 2008. Biogeography-based optimization: *IEEE transactions on evolutionary*
723 *computation* 12, 702-713. <https://doi.org/10.1109/TEVC.2008.919004>.
- 724 Storn, R., Price, K., 1997. Differential evolution—a simple and efficient heuristic for global
725 optimization over continuous spaces. *Journal of global optimization* 11, 341-359.
726 <https://doi.org/10.1023/A:1008202821328>.
- 727 Whitley, D., 1994. A genetic algorithm tutorial, *Statistics and Computing* 4, 65-85.
728 <https://doi.org/10.1007/BF00175354>.



729 Yang, X.S., 2010. A new metaheuristic bat-inspired algorithm. In nature inspired
730 cooperative strategies for optimization (NICSO 2010), Springer, Berlin, Heidelberg.
731 65-74. https://doi.org/10.1007/978-3-642-12538-6_6.